



Supplement of

15-year variability of desert dust optical depth on global and regional scales

Stavros-Andreas Logothetis et al.

Correspondence to: Andreas Kazantzidis (akaza@upatras.gr)

The copyright of individual parts of the supplement might differ from the article licence.

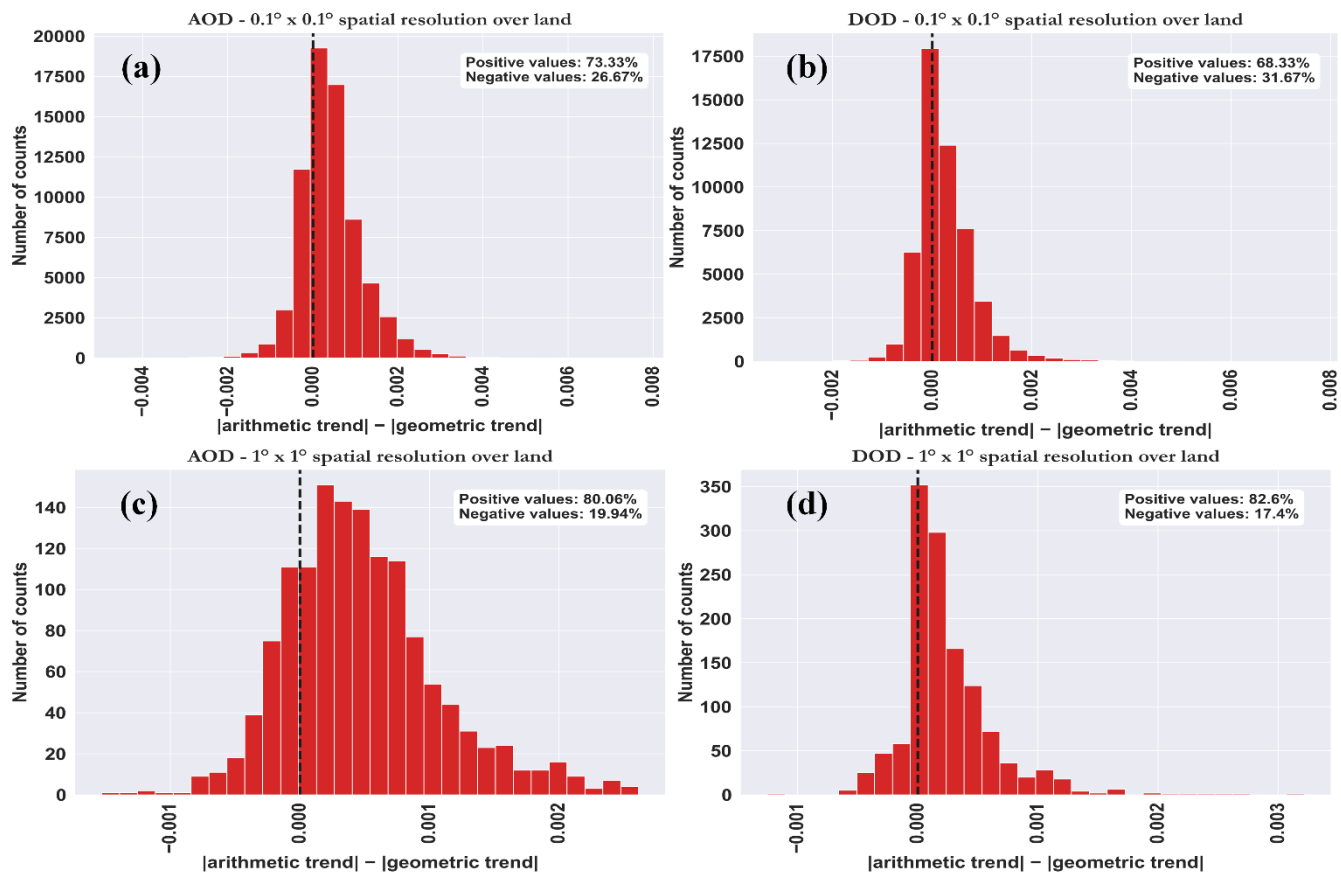


Figure S1: Histograms showing the differences between geometric-based and arithmetic-based trends for (a) AOD and (b) DOD at $0.1^\circ \times 0.1^\circ$ and (c) AOD and (d) DOD at $1^\circ \times 1^\circ$ over land.

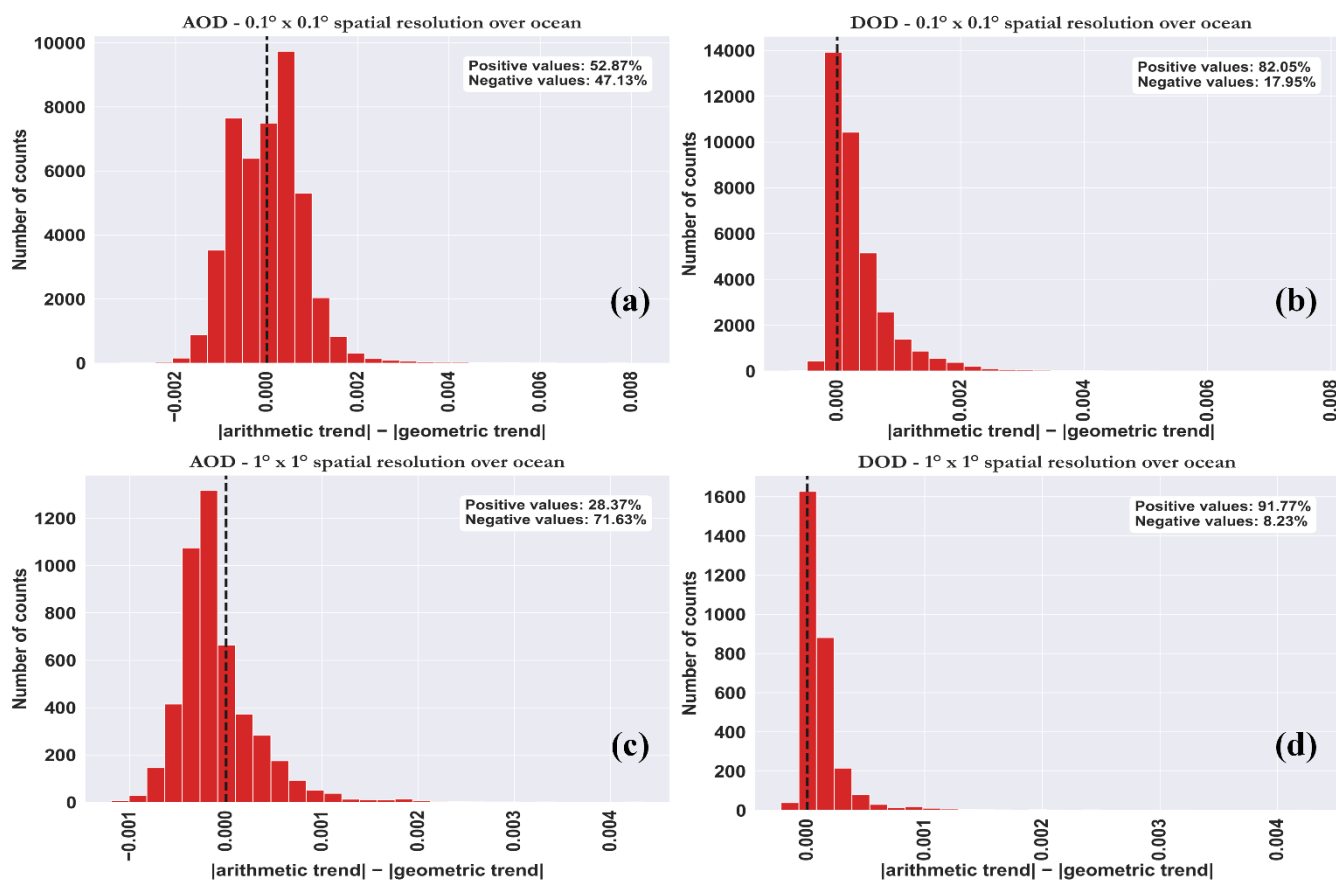
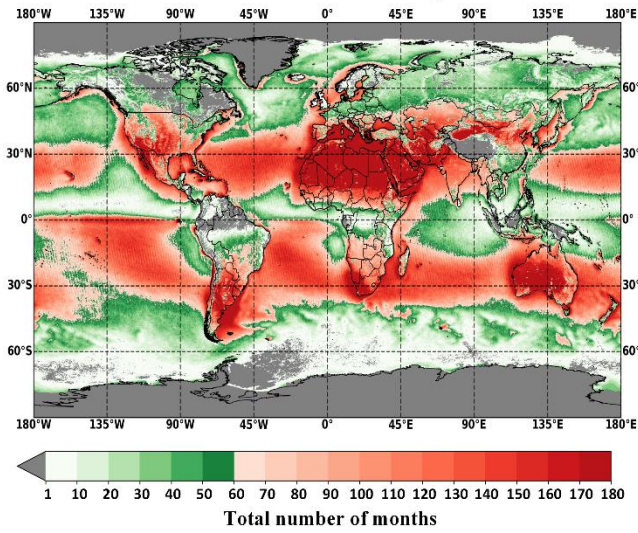


Figure S2: Same as Fig. S1 over ocean.

(a) Total number of months at $0.1^\circ \times 0.1^\circ$ spatial resolution



(b) Total number of months at $1^\circ \times 1^\circ$ spatial resolution

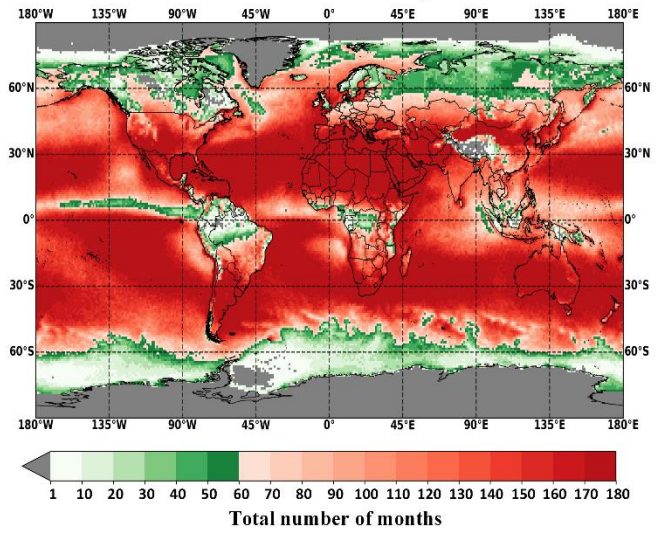


Figure S3: Global distribution of total number of months at (a) $0.1^\circ \times 0.1^\circ$ and (b) $1^\circ \times 1^\circ$ spatial resolution. The pixels with not available data are colored with gray color while those of failing to meet the availability criteria (see Sect. 2.3) are colored with greenish.

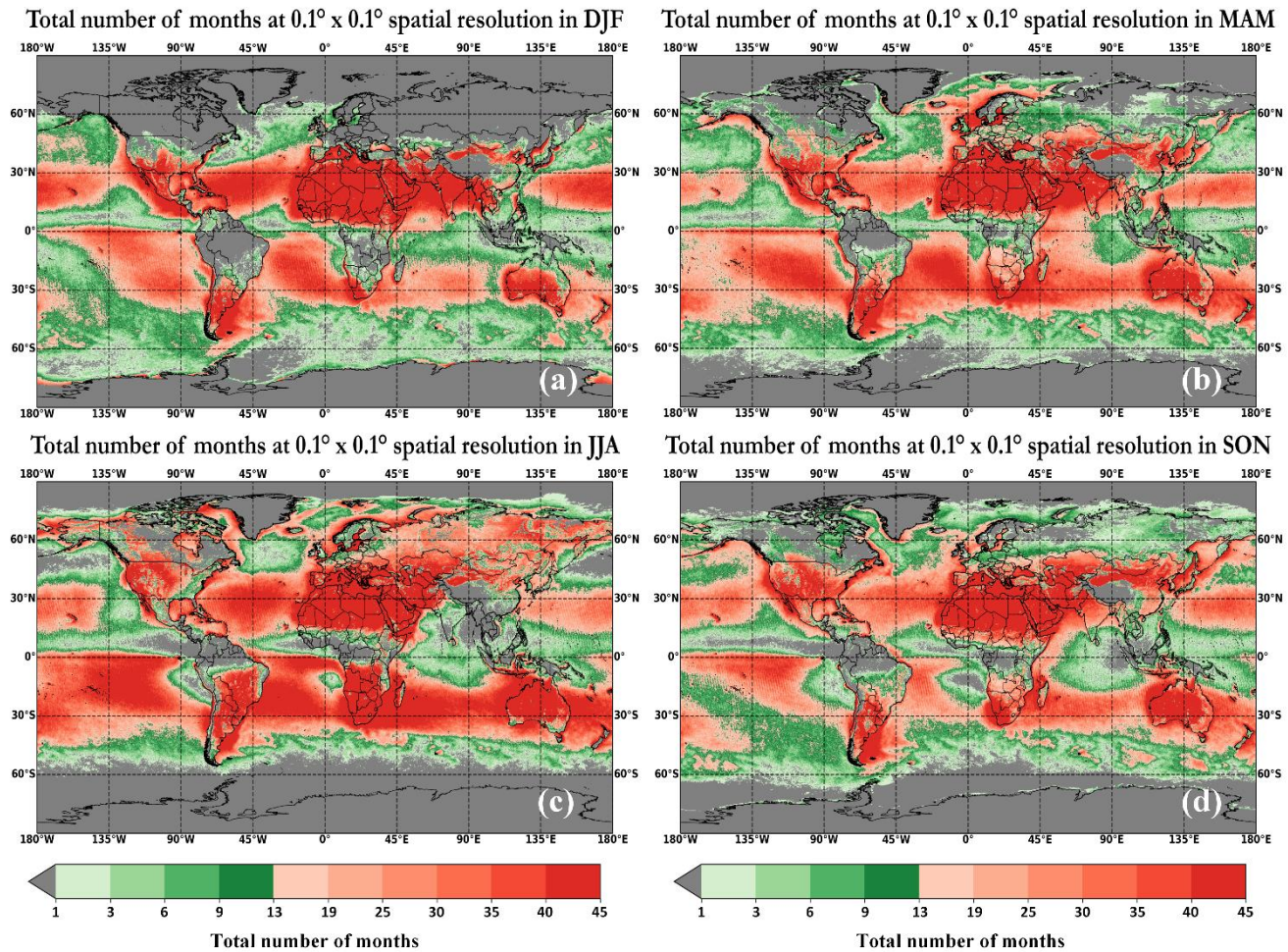


Figure S4: Total number of months at (a) December-January-February (DJF), (b) March-April-May (MAM), (c) June-July-August (JJA), and (d) September-October-November (SON) at $0.1^\circ \times 0.1^\circ$ spatial resolution.

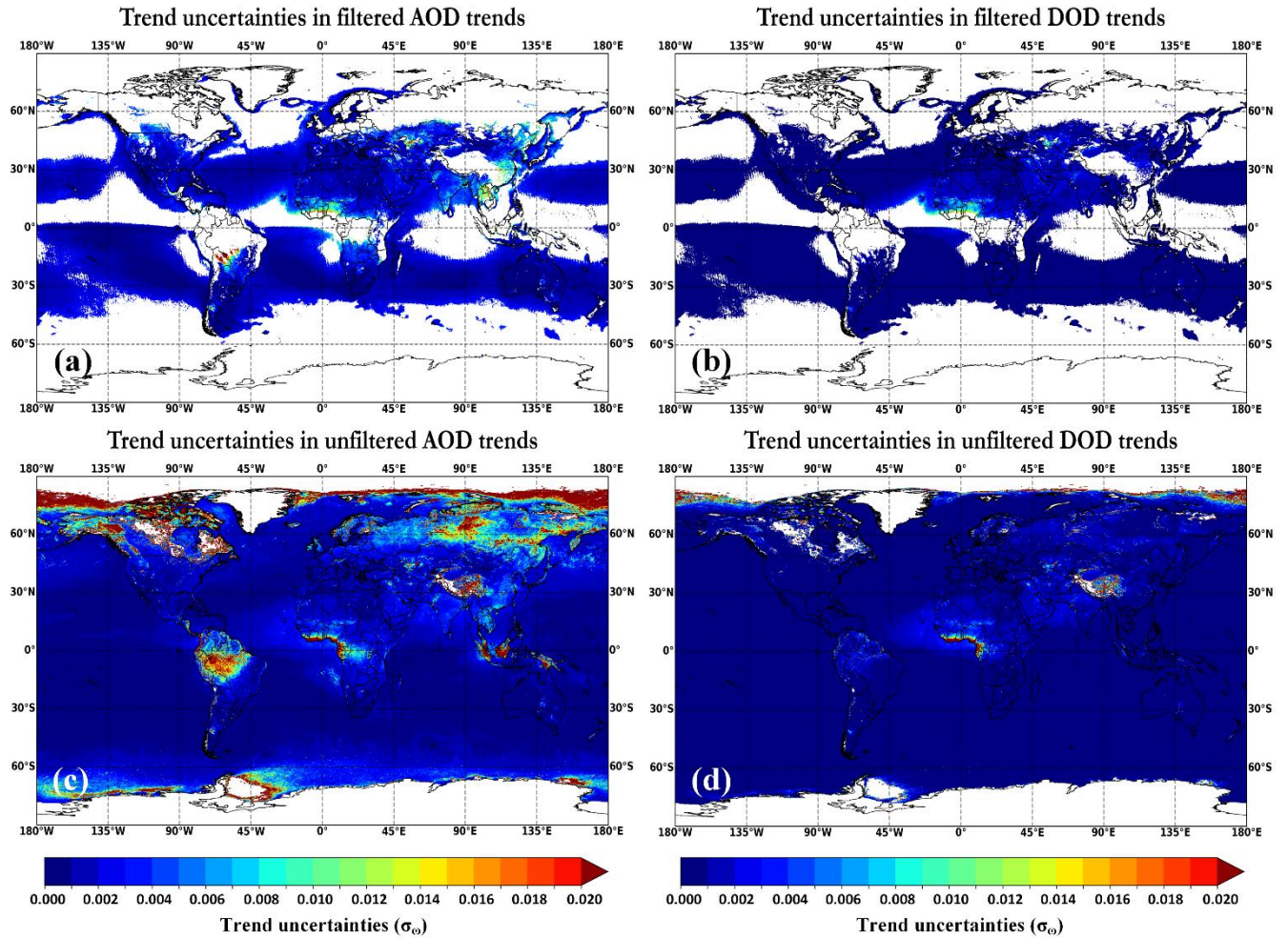


Figure S5: Global maps of temporal trends uncertainties, at $0.1^\circ \times 0.1^\circ$ spatial resolution, using Eq. (3) for AOD (a and c) and DOD (b and d). Upper panel (a, b) shows the filtered trends uncertainties (based on Fig. 2c, d trends) while the bottom panel (c, d) indicates the unfiltered trends uncertainties (based on Fig. 5a, b trends).

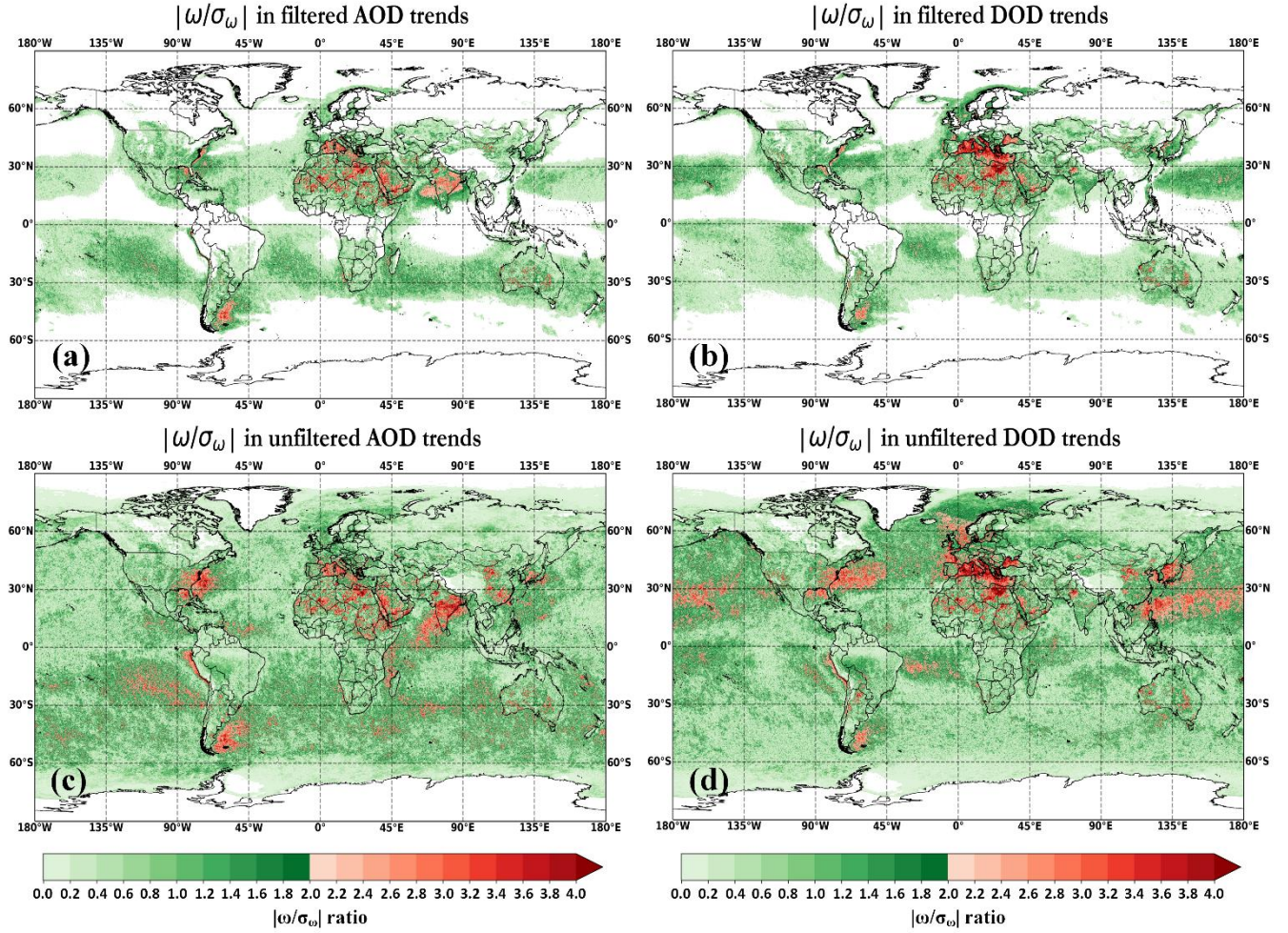


Figure S6: Global maps of $|\omega/\sigma_\omega|$ ratio, at $0.1^\circ \times 0.1^\circ$ spatial resolution, using Eq. (3) for AOD (a and c) and DOD (b and d). Upper panel (a, b) shows the filtered trends $|\omega/\sigma_\omega|$ ratio (based on Fig. 2c, d trends) while the bottom panel (c, d) indicates the unfiltered trends $|\omega/\sigma_\omega|$ ratio (based on Fig. 5a, b trends).

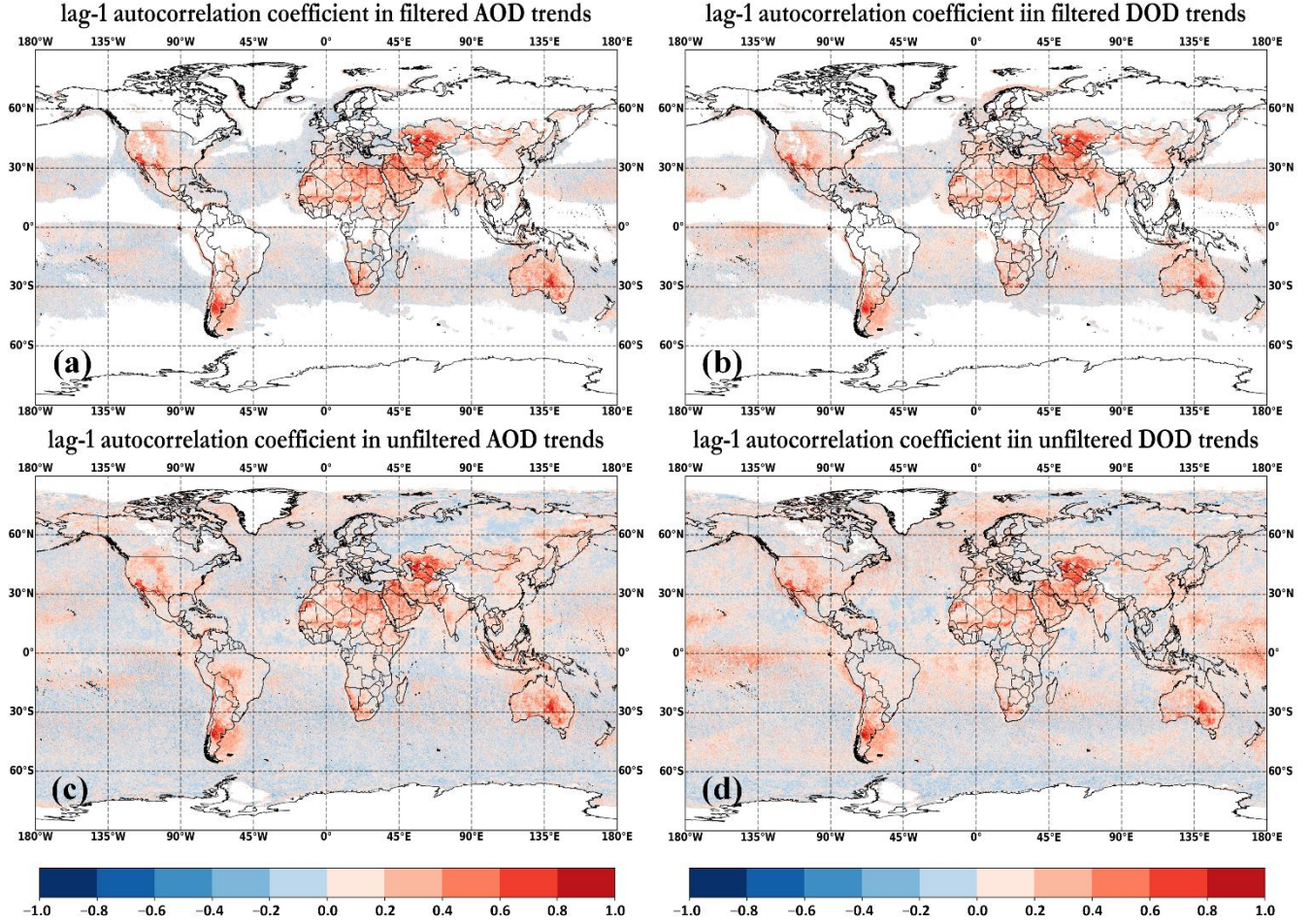


Figure S7: Global maps of lag-1 autocorrelation coefficient, at $0.1^\circ \times 0.1^\circ$ spatial resolution, using Eq. (3) for AOD (a and c) and DOD (b and d). Upper panel (a, b) shows the filtered trends of lag-1 autocorrelation coefficient (based on Fig. 2c, d trends) while the bottom panel (c, d) indicates the unfiltered trends of lag-1 autocorrelation coefficient (based on Fig. 5a, b trends).

Differences in data availability between unfiltered and filtered trend analysis

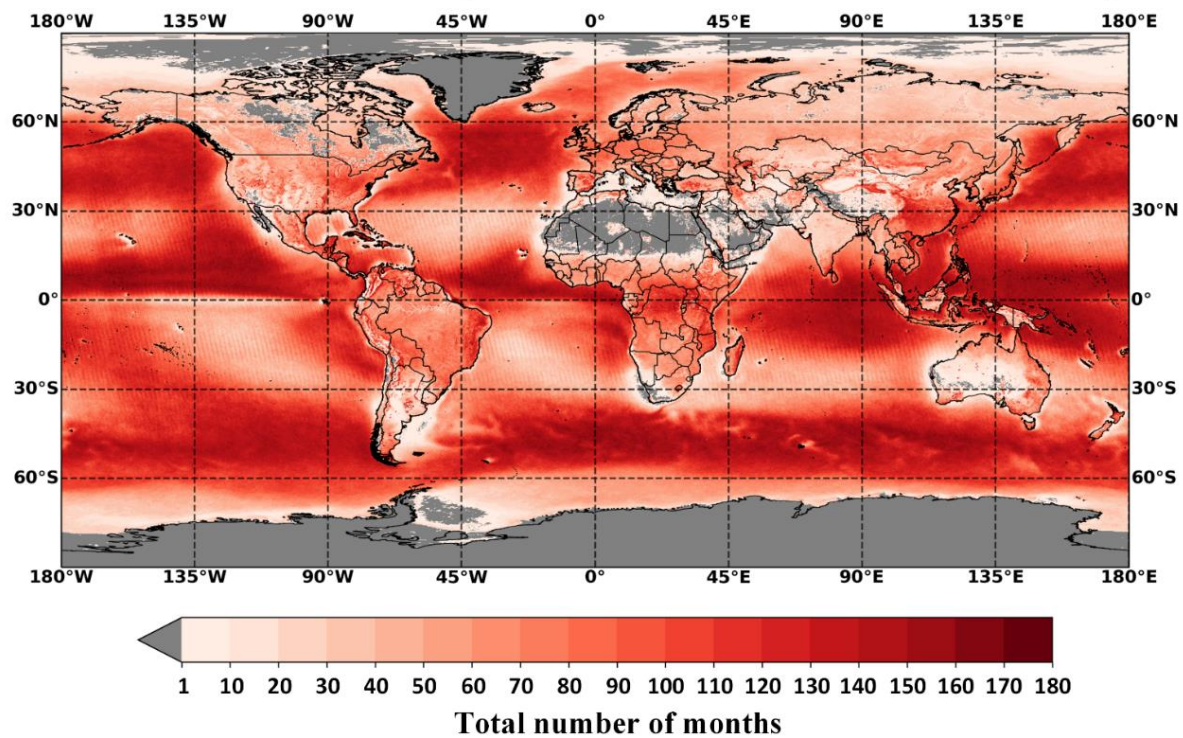


Figure S8: Differences in total number of months between the unfiltered (Fig. 5) and filtered (Fig. 2) trend analysis.

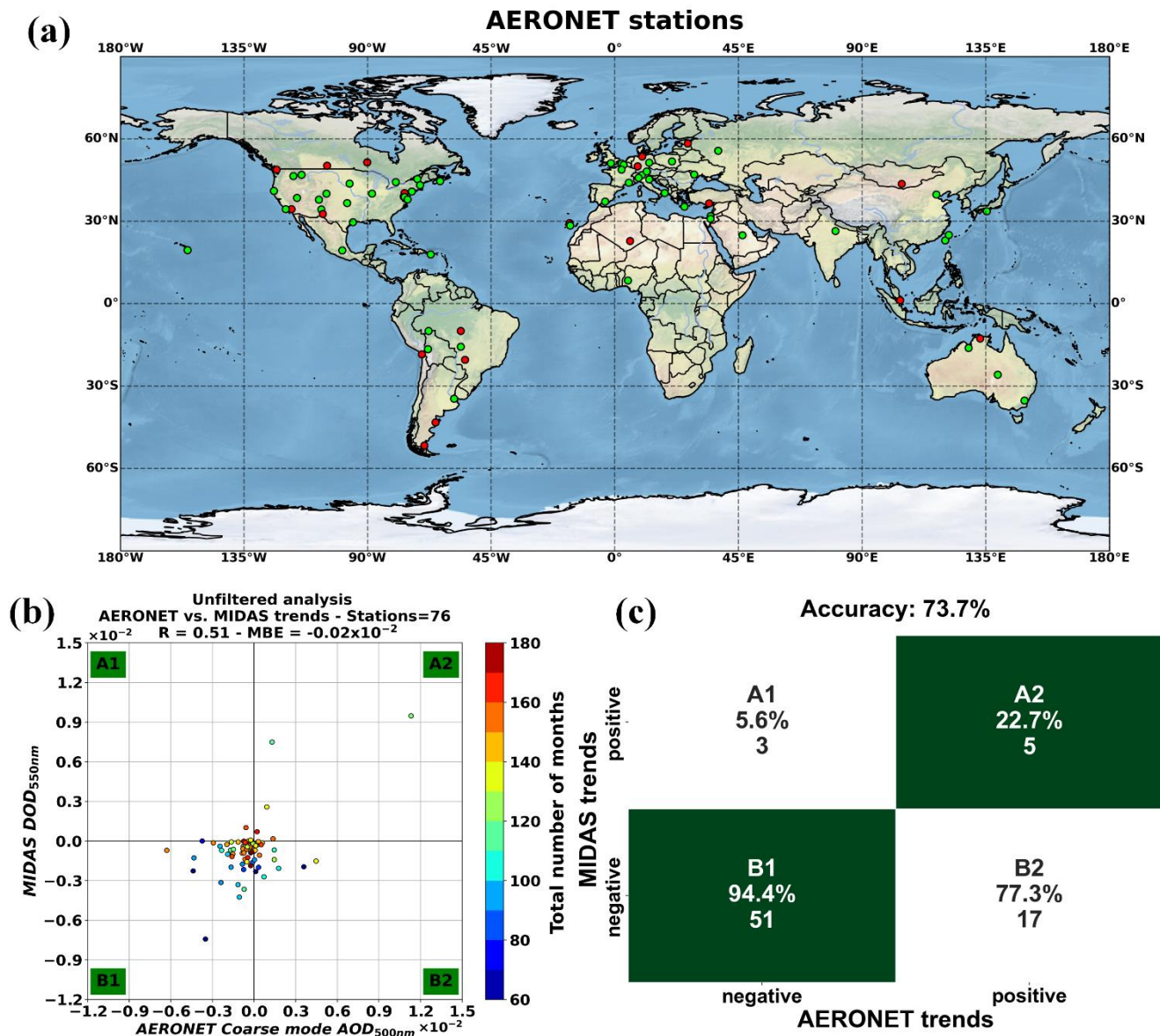


Figure S9: Same as Fig. 4 for unfiltered trend analysis.

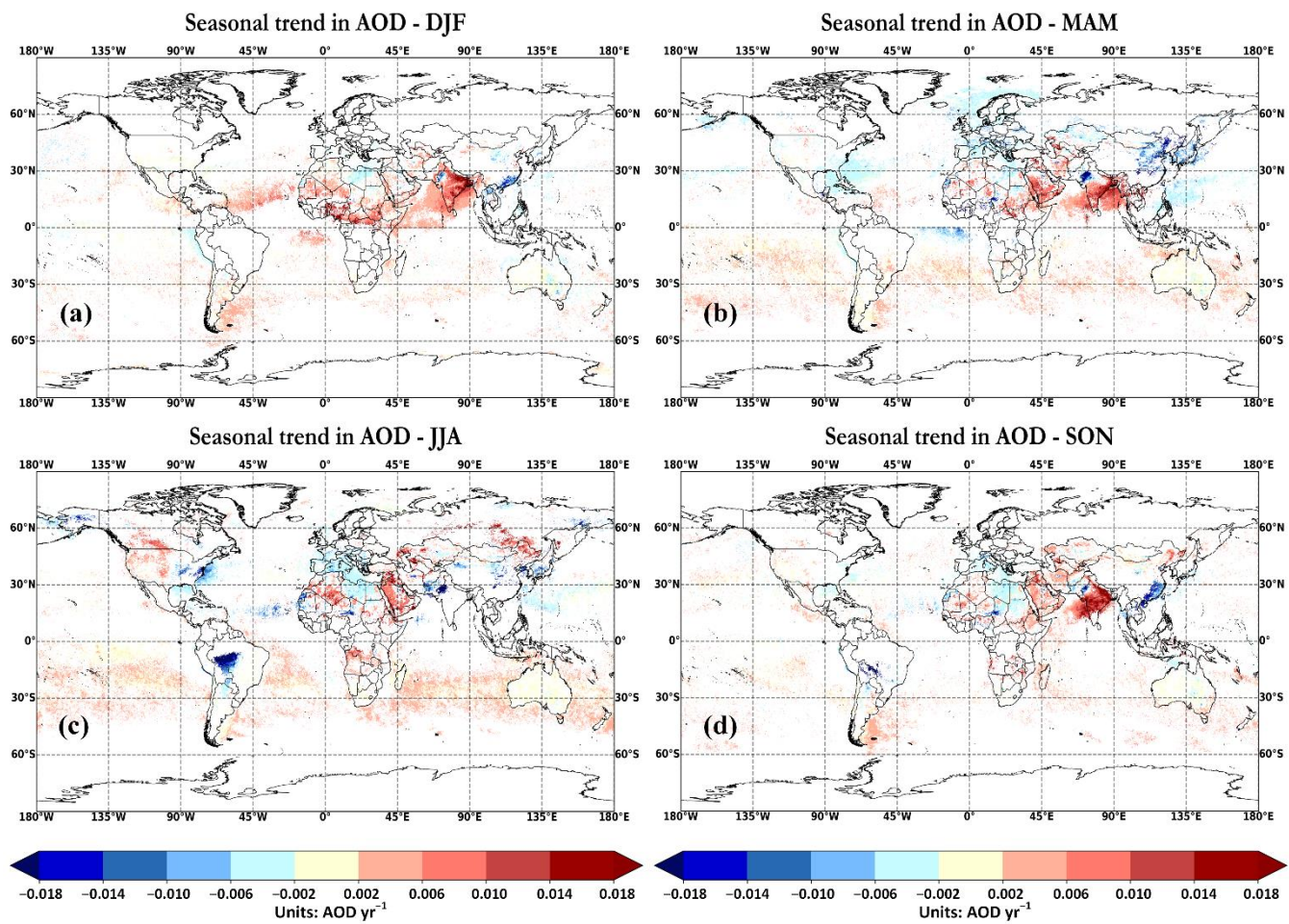


Figure S10: Same as Fig. 6 for AOD.

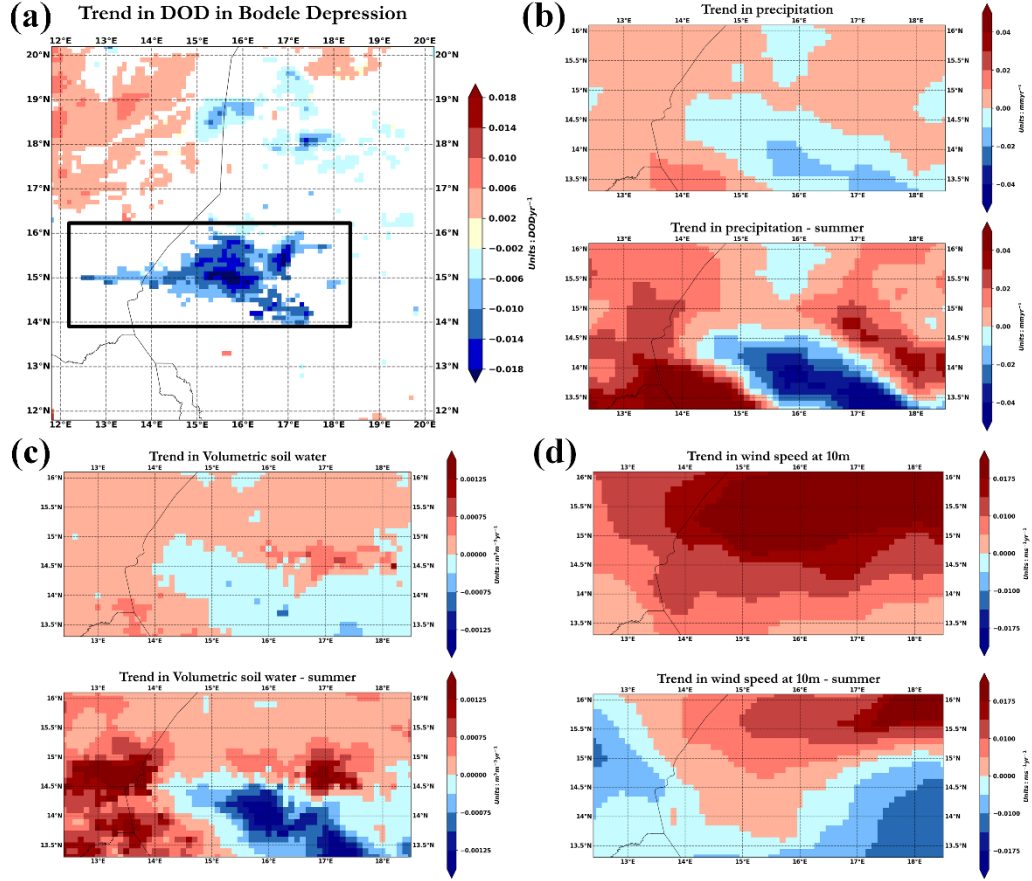


Figure S11: Geographical distribution of long-term (a) DOD trends, and long-term along with summertime trends of (b) total precipitation, (c) volumetric soil water and (d) wind speed at 10m across Bodélé Depression. All the applied parameters are retrieved from ERA5 reanalysis dataset (<https://www.ecmwf.int/en/forecasts/datasets/reanalysis-datasets/era5>).

Table S1: Regional trends between MIDAS DOD and AERONET coarse mode AOD. N refers to total number of MIDAS-AERONET months where the trends are calculated. The star symbols corresponds to statistically significant regions under the 95% (*) and 90% (**) confidence level. Additional information about AERONET stations can be retrieved by <https://aeronet.gsfc.nasa.gov/>. Green and red color refers to the stations with the similar and different trends sign, respectively.

trends $\times 10^{-2} \text{ yr}^{-1}$									
Station	AERONET	MIDAS	N	Period	Station	AERONET	MIDAS	N	Period
Arica	0.019	-0.014	83	2003–2017	MD_Science_Center	0.0937	-0.2469*	83	2004–2017
Birdsville	-0.011	-0.108	106	2005–2017	Moldova	-0.0280	-0.0896	106	2003–2017
BONDVILLE	-0.121	-0.054	61	2003–2017	Nes_Ziona	0.0052	-0.0823	61	2003–2017
BSRN_BAO_Boulder	-0.095**	-0.053	95	2003–2016	Railroad_Valley	-0.0272	-0.1243*	95	2003–2017
Canberra	-0.083*	-0.002	111	2003–2017	Rimrock	-0.0555	-0.1276*	111	2003–2017
Carpentras	-0.037	-0.182*	107	2004–2017	Santa_Cruz_Tenerife	0.1418	0.0350	107	2003–2015
CART_SITE	0.009	-0.026	134	2003–2017	SEDE_BOKER	-0.0377	-0.1920	134	2003–2017
CEILAP-BA	0.081	0.200*	74	2003–2017	SERC	-0.2279*	-0.1983*	74	2003–2017
CUIABA-MIRANDA	-0.224	-0.048	71	2003–2017	Sevilleta	-0.0819*	-0.0176*	71	2005–2017
Dalanzadgad	0.093	0.022	90	2003–2017	Shirahama	-0.2022	-0.1248	90	2003–2017
FORTH_CRETE	-0.021	-0.184	94	2003–2017	Sioux_Falls	-0.0938	-0.1799*	94	2003–2017
Granada	-0.080	-0.447**	70	2005–2017	Solar_Village	1.2559**	1.0739	70	2003–2017
GSFC	-0.028	-0.150*	109	2003–2017	TABLE_MOUNTAIN_CA	-0.0238	-0.0681	109	2003–2017
IMS-METU-ERDEMLI	-0.064	-0.191**	115	2004–2017	Tamanrasset_INM	0.6188**	0.4369	115	2004–2017
Ispira	-0.133	-0.152*	92	2003–2017	Trelew	0.0640	0.0001	92	2003–2013
Izana	-0.059	0.0006	71	2004–2017	Trinidad_Head	-0.3544**	-0.1194*	71	2006–2017
Jabiru	-0.097	0.012	73	2003–2017	UCSB	-0.0203	-0.1900*	73	2006–2017
Kanpur	-0.268	-0.292	122	2003–2017	Venise	-0.0203	-0.1100*	122	2005–2017
La_Parguera	0.1514	0.3521**	70	2004–2017	White_Sands_HELSTF	-0.0368	0.0171	70	2005–2017
Lake_Argyle	-0.0779	0.0078	113	2003–2017	XiangHe	-0.2788*	-0.1844	113	2003–2017
Lecce_University	-0.0233	-0.0195	105	2003–2017					